

Article

An Optimized Approach for Serial Crystallography Using Chips

Marina Galchenkova ¹, Aida Rahmani Mashhour ¹, Patrick Y. A. Reinke ¹, Sebastian Günther ¹, Jan Meyer ¹, Henry N. Chapman ^{1,2,3} and Oleksandr M. Yefanov ^{1,*}

¹ Center for Free-Electron Laser Science CFEL, Deutsches Elektronen-Synchrotron DESY, Notkestrasse 85, 22607 Hamburg, Germany; marina.galchenkova@desy.de (M.G.)

² Department of Physics, Universität Hamburg, Luruper Chaussee 149, 22761 Hamburg, Germany

³ The Hamburg Center for Ultrafast Imaging, Universität Hamburg, Luruper Chaussee 149, 22761 Hamburg, Germany

* Correspondence: oleksandr.yefanov@desy.de

Abstract: Serial crystallography is a rapidly developing method for the determination of the structure of biomolecules at room temperature at near-atomic resolution from an ensemble of small crystals. Numerous advances in detectors, data analysis pipelines, sample delivery methods, and crystallization protocols expand the scope of structural biology to understand the fundamental processes that take place in living cells. Many experimental strategies for serial crystallography are in use, depending on the type and sizes of the crystals or other needs of the experiment. Such strategies should ideally minimize the wastage of samples or beamtime without compromising experimental goals. This paper proposes a way to optimize beamtime utilization in serial crystallography experiments that use fixed-target sample delivery methods, such as chips. The strategy involves two key steps. Firstly, a fast raster scan of the chip is performed to determine the positions of the crystals based on their diffraction. Subsequently, a rotational series is collected at each identified crystal position, covering a narrow range of chip orientations. This approach enables the exclusion of empty positions during data acquisition, resulting in significant savings in beam time utilization and a reduced volume of measured data.

Keywords: serial crystallography; fixed-target sample delivery; hit-rate optimization; chip scanning



Citation: Galchenkova, M.; Rahmani Mashhour, A.; Reinke, P.Y.A.; Günther, S.; Meyer, J.; Chapman, H.N.; Yefanov, O.M. An Optimized Approach for Serial Crystallography Using Chips. *Crystals* **2023**, *13*, 1225. <https://doi.org/10.3390/cryst13081225>

Academic Editor: Francesco Stellato

Received: 30 June 2023

Revised: 4 August 2023

Accepted: 6 August 2023

Published: 9 August 2023



Copyright: © 2023 by the authors. Licensee MDPI, Basel, Switzerland. This article is an open access article distributed under the terms and conditions of the Creative Commons Attribution (CC BY) license (<https://creativecommons.org/licenses/by/4.0/>).

1. Introduction

The 3D structures of proteins can be observed at the atomic scale by the method of X-ray crystallography. In macromolecular crystallography, the conventional approach involves acquiring diffraction patterns from a crystal while it undergoes rotation along one or more axes. The total tolerable X-ray exposure of the crystal is limited by the accumulation of damage to the protein structure by ionizing radiation [1,2]. Cryogenic cooling reduces the processes of radiolysis and extends the exposure that can be tolerated. However, such cooling may alter the macromolecular structure and prevent the ability to measure dynamic processes by time-resolved methods [3].

Recently, the method of serial crystallography (SX) has been developed at synchrotron radiation facilities and X-ray free-electron lasers (FELs) to overcome this limitation [3–7]. In contrast to the conventional rotation method, in SX, a large number of randomly oriented crystals are sequentially exposed to an X-ray beam, one at a time. This random orientation of crystals leads to the collection of numerous snapshot diffraction patterns to obtain a complete set of 3D structure factors in a stochastic manner. A notable advantage of serial crystallography is the ability to apply the full tolerable X-ray exposure to each individual crystal, as opposed to distributing it across a rotation series of a single crystal. This approach can avoid the need for cryogenic cooling. Serial crystallography conducted at synchrotron or free-electron laser (FEL) sources offers a powerful approach to unraveling the

dynamics of structural fluctuations and investigating the mechanisms of macromolecules. By obtaining protein structures at multiple time points, this technique provides valuable insights into the dynamic behavior of biomolecules [8,9].

Various sample delivery systems have been employed or investigated for delivering micro- to nanoscale crystalline samples into the X-ray beam [10,11]. The choice of the most suitable sample delivery method depends on the experimental goals, the required environment, and the characteristics of the crystals (such as size or quantity). One class of methods generates a free jet of a liquid suspension of crystals [12,13] that flows continuously across the X-ray beam and a diffraction pattern is acquired at each X-ray pulse or exposure, whether the beam intersects a crystal or not. Variations include slowly flowing extrusions of crystals in a viscous medium [14] or transporting the suspension as drops applied to a moving tape [15].

A conceptually different approach is to deposit crystals onto a solid supporting membrane, which is then raster scanned in the X-ray beam [16]. These “fixed-target” sample delivery systems encompass patterned silicon chips [17–23] or plastic membranes [24–26]. This approach also facilitates on-the-chip crystallization [27], making it more suitable for fragile crystals that might otherwise suffer damage from injection-based methods. To mitigate potential crystal orientation biases, the support can be rotated within the X-ray beam. Data collection can be carried out either at room temperature with controlled humidity or at cryogenic temperatures. Some beamlines incorporate a robot to mount holders on the goniometer, eliminating the need to access the experimental hutch during the experiment.

Recent years have witnessed the development of several distinct fixed-target designs for serial crystallography. A class of these uses a thin membrane chip, made of silicon or silicon nitride, with periodic microscopic wells or pores [16–21] (Figure 1). When appropriately sized, pores may trap the crystals when excess mother liquor is removed via blotting [21], resulting in minimal background scattering in the diffraction pattern [20,22,23]. To prevent crystal dehydration, the chip is commonly sealed between two membranes or maintained in a humid environment, such as a stream of humidified gas. The former scheme is suitable for vacuum measurements, while the latter offers the advantage of lower background by avoiding the introduction of additional material into the X-ray beam.

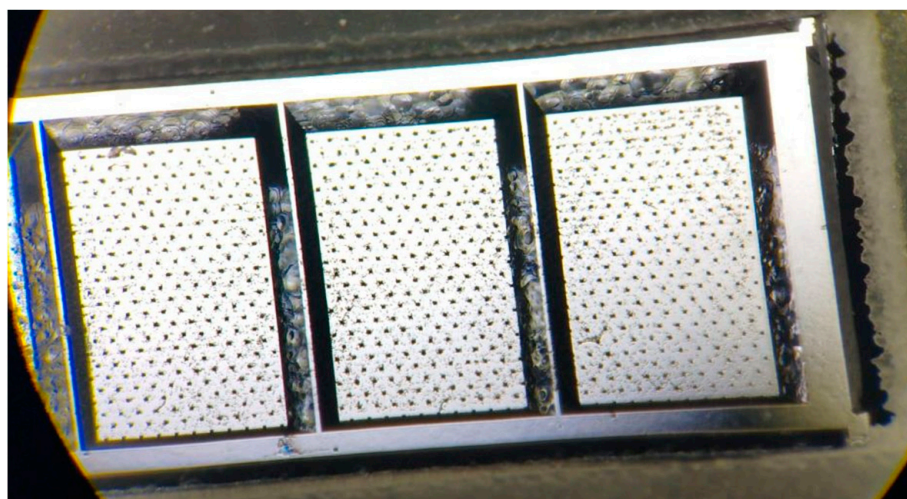


Figure 1. A photo of used $4 \times 10 \text{ mm}^2$ silicon chips, manufactured by Suna Precision (<https://www.suna-precision.com/products/serial-crystallography/silicon-chips>, accessed on 1 August 2023).

An advantage of the fixed-target rastering approach, which we capitalize on in this work, is that it provides the possibility to measure every individual crystal, to efficiently utilize the protein and reduce sample consumption. This is beneficial for protein samples that are expensive to produce. Furthermore, if the positions of the crystals are known before data collection, it is possible to measure only at those positions and achieve efficient use of the X-ray beam. Moreover, each crystal small rotation series can be measured, which proves to be beneficial in mitigating the partiality problem [28]. As mentioned above, crystals can be placed into well-defined locations determined by the pore structure of the chip or found by inspection before the X-ray measurements no matter where they are located [19]. The primary challenge associated with loading crystals into pores or wells is that they, particularly larger crystals, may not always be confined to those specific positions and can be distributed anywhere on the chip. Additionally, smaller crystals that are smaller than the pore size might be lost during the blotting process. The measurement of crystal locations can be achieved in different ways: via UV tryptophan fluorescence imaging [29–31], UV-vis spectroscopy [19,32], second-order nonlinear imaging of chiral crystals (SONICC) [33], or even manually selecting crystals using an in-line visible microscope [20,34]. In the case of SONICC microscopy, it was found that microcrystal positions could be determined with a spatial resolution of approximately 2 μm with fast image acquisition times, in correlation with the crystal locations identified by raster scanning using an X-ray beam [33]. Using UV-vis spectroscopy to predetermine crystal locations in fixed-target room-temperature crystallography [19], an exceptional performance was demonstrated with a raw hit rate of nearly 100% and an effective indexing rate of approximately 50%. Unfortunately, all these methods have their limitations: SONICC has not been integrated at beamlines, optical auto-search of crystal positions may fail since the crystals have very different shapes and sizes, while manual centering requires a lot of concentration and user intervention.

To improve the data collection with fixed-target sample delivery we propose a two-stage scanning protocol for the chip: first, a fast fly scan (measuring during the movement) is made to find positions of the chip with diffracting crystals, followed by a mini-rotation series (scanning over 1–5 degrees) only at each of those found positions with crystals (Figure 2). In practice, it is implemented in the following way: the fly scan is performed with a low fluence X-ray beam and at the maximum scanning speed to limit the exposure and prevent damage to the crystals. The collected data are then analyzed to determine the positions of the chip at which the crystal diffraction was observed. A data analysis process is initiated in parallel after each row of the raster scan to provide results shortly after the full scan has finished. Then, at each scan position where crystal diffraction was detected (according to some criterion, such as the presence of a certain number of Bragg peaks), a rotation series is collected over a small range of angles while not exceeding the total tolerable dose. Such an approach speeds up the data collection and reduces the total data volume collected. Due to the fact that pre-scanning is performed in the same configuration as the actual data acquisition, the chances to miss some crystals or to scan non-crystalline samples are rather low.

Here, we present a proof of principle of this “smart” X-ray chip scanning by introducing the intermediate step of crystal localization into the CrystalControl software developed at the P11 beamline of the PETRA III synchrotron radiation facility in Hamburg, DESY.

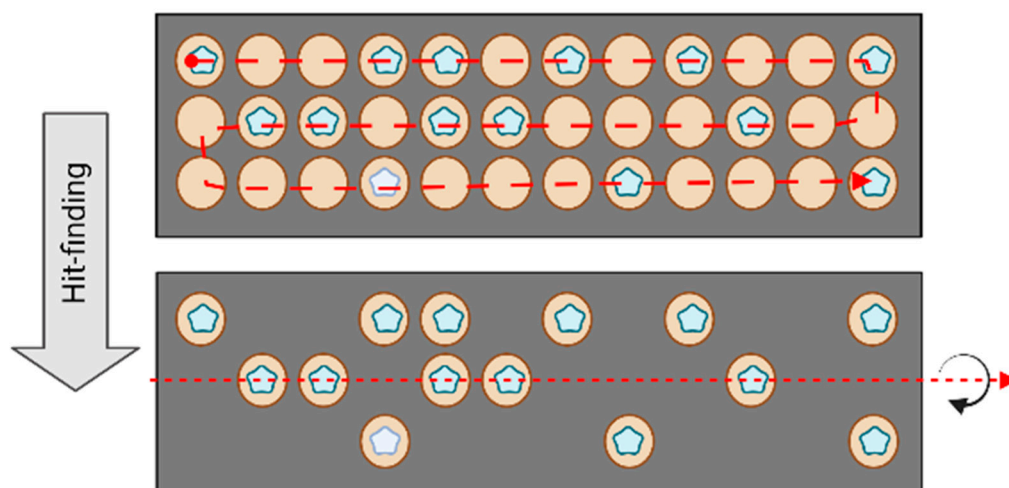


Figure 2. The principle of the smart chip-scanning approach. First, an on-the-fly scan is performed to locate well-diffracting protein crystals and then mini-rotation series were measured at each detected crystal position.

2. Materials and Methods

For our demonstration experiments at the P11 beamline of the PETRA III synchrotron radiation facility, we used $4 \times 10 \text{ mm}^2$ silicon chips, manufactured by Suna Precision [18] (see Figure 1), covered by a suspension of lysozyme crystals.

2.1. Sample Preparation

The following protocol for sample crystallization was used [27]: hen egg white lysozyme was purchased from Sigma-Aldrich and dissolved in 50 mM sodium acetate pH 3.5 (140 mg/mL) and filtered through a $0.2 \mu\text{m}$ filter. A cold solution ($4 \text{ }^\circ\text{C}$) of 60 mg/mL lysozyme was mixed 1:1.5 with a prechilled ($4 \text{ }^\circ\text{C}$) precipitation solution (50 mM sodium acetate pH 3.5, 0.75 M sodium chloride, 30% ethylene glycol, 11.25% polyethylene glycol 400), adapted from Lieske et al., 2019. The mixture was incubated at $4 \text{ }^\circ\text{C}$ for 16 h and mixed at intervals using an Eppendorf Thermomixer C (1600 rpm for 30 s, every 5 min). Crystals ranging in size from $25 \mu\text{m}$ to $40 \mu\text{m}$ were obtained, with a mean size of $30 \mu\text{m}$.

2.2. Experimental Setup and Data Collection

A micro-patterned silicon chip (Suna Precision, Hamburg, Germany) with a size of $4 \times 10 \text{ mm}^2$ was used as a fixed-target sample holder [18]. The silicon chip was perforated with a regular array of $25 \mu\text{m}$ square holes through which excess liquid can be blotted. The silicon chip holder has a cavity that serves as a mother liquor reservoir and provides an equilibrated humid environment for the sample during the measurements. Lysozyme crystals were deposited on the chip and the excess reservoir solution was blotted through the chip holes with a tissue. A thin mylar foil sleeve was used to retain humidity and prevent the sample from drying out.

The chip was manually mounted on the goniometer using the standard magnetic mount. The alignment of the chip is performed using the in-line microscope to make sure that the center of rotation stays at the chip for any position within the scan. The diffraction measurements were carried out at a photon energy of 18 keV using an Eiger 2X 16M detector placed 155 mm behind the sample, and the beam was focused to a spot of $9 \times 5 \mu\text{m}^2$. The flux of the unattenuated beam was 5×10^{12} ph/s.

The P11 goniometer and data acquisition process is controlled through a custom Python-based graphical user interface (GUI) called CrystalControl (CC) [35]. In addition to the conventional data acquisition modes for macromolecular crystallography (MX), this GUI offers various features specifically designed for micro-crystallography, such as a grid scanning capability. The grid can cover the entire chip or a specific area of interest

(one region of interest per data collection). The user has the capability to draw a grid directly onto the image from the in-line microscope. Two modes for grid scans are implemented in CC: fly scan, where measurements are taken during the horizontal movement of the chip, and step scan, where the chip is first shifted to a position and then the measurement is performed. In our protocol, we implemented a two-step process for data collection. Firstly, we conducted a low-dose finder scan using the fly scan method. The obtained results from this finder scan were processed using the method described below to identify the positions on the grid where crystal diffraction was detected. Subsequently, we modified the step scan to sequentially visit the determined positions for actual data collection.

The maximum speed of the fly scan, used for hit finding, is ultimately limited by the detector frame rate of 133 Hz (7.5 ms exposure). In practice, the speed is often limited by the speed of the goniometer movement and, thus, large steps usually require a longer acquisition time, which is then coupled with a reduced beamline transmission. For example, with an exposure time of 40 ms, a step size of 50 μm , and 1% beamline transmission, this hit-finding scan delivered a dose of 1.3 kGy to each lysozyme crystal. In the fly scan mode, the measurements are performed at a fixed orientation of the chip.

2.3. Data Analysis

We used and compared two hit-finding algorithms, peakfinder8 [36] and Dozor [37]. Peakfinder8 finds frames with Bragg peaks by identifying regions in the diffraction pattern consisting of a specific number n of connected pixels ($n_{\min} \leq n \leq n_{\max}$) with intensity values above a threshold determined from the radially averaged background intensity. A pattern is considered a hit when the number of regions found, each exhibiting a sufficiently high signal-to-noise ratio, exceeds a predetermined minimum value of N_{peaks} . Each horizontal line of the grid during the fly scan is saved as a separate HDF5 file, so, as soon as the file was saved, the hit-finding analysis was started. To speed up the calculations, the processing of each scanned line was submitted as a job to the DESY Maxwell HPC Cluster (<https://confluence.desy.de/display/IS/Maxwell>, accessed on 1 August 2023). Since the Maxwell cluster contains many powerful nodes, this strategy performs hit-finding almost in real time.

The Dozor program [37] was also executed for each line separately on the dedicated P11 cluster. The algorithm for finding the Bragg peaks used in Dozor is quite similar to the one used in peakfinder8, with some differences in the statistics calculation and the implementation [37]. The hit-finding programs provide the positions of the substrate where the beam intersects crystals. A comparison of the crystal positions determined by the two programs is given in Figure 3. These co-ordinates were then saved, but the diffraction frames recorded during the fly scan could be ultimately discarded.

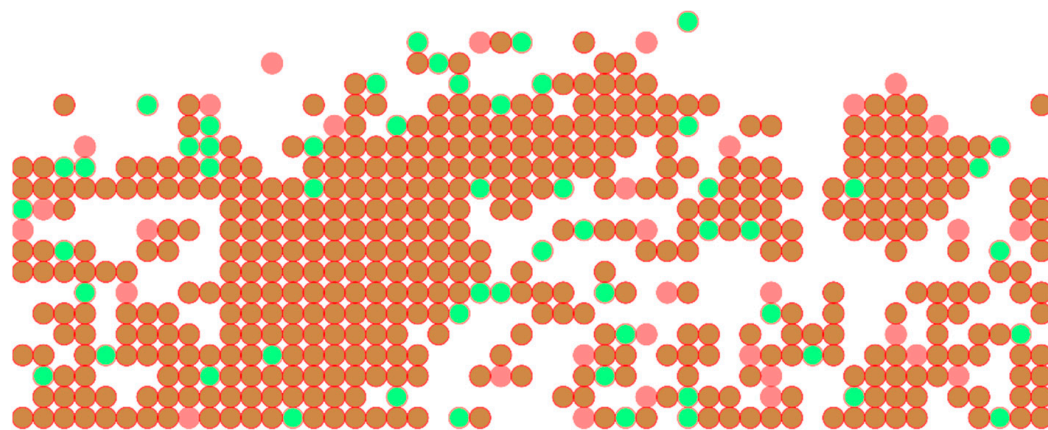


Figure 3. The positions of detected protein crystals by peakfinder8 (pink) and Dozor (green).

After the hit finding, the modified grid (excluding positions where no crystal diffraction was recorded) was loaded into the step scan. In a typical step scan, the chip was shifted to each occupied position of the grid, where a rotation mini-series was performed, consisting of 11 frames, 0.36 degrees/frame. The beamline transmission was set to 10% and the exposure per frame was 100 ms (an exposure 25 times larger than the initial scan). This measurement deposited a dose of 326 kGy, which can be considered tolerable [38].

The data collected using small rotation series at the positions of the found crystals were further processed using CrystFEL 0.10.1. The peakfinder8 algorithm was used for identifying the Bragg peaks with parameters: --min-snr=4, --threshold=5, --min-pix-count=2, --max-pix-count=20. We want to note here that the parameter “max-pix-count” helps to discard the Bragg peaks produced by the silicon chip. Detected “hits” were indexed using Xgandalf [39] and using --no-cell-combinations --no-check-peaks --muti options and integrated with --int-radius=2,4,6. Small rotational series of lysozyme from two experiments were scaled and merged into group 4/mmm using xsphere as the partiality model by executing the partialator in CrystFEL, using three iterations and --push-res=1.0. Figures of merit (SNR, Completeness, R_{split} , and CC^*) were calculated using compare_hkl and check_hkl, all part of the CrystFEL package, with --highres=2.0 --nshells=20 options. MTZ files for crystallographic data processing were generated from CrystFEL merged reflection datafiles using F2MTZ of the CCP4 program suite.

The structure refinement of processed data was performed with phenix.refine [40] (Phenix/1.20) with such parameters as xray_data.high_resolution=2.0 and xray_data.low_resolution=20, using 6FTR as the search model. The results are presented in the next section.

3. Results

To demonstrate the results of the proposed approach, three examples of scanned chips are shown in Figure 4. The images were recorded using the in-line microscope at the beamline, for which the magnification and position are calibrated relative to the scanning stage. In each case, the green rectangle was set to define the range of the finder scan, and the fly-scan parameters determine the number of rows and columns in the grid. The green circles show the locations of crystal diffraction hits. It is notable that these locations do not correlate with the positions of the square-shaped pores in the chips, nor with visible features that might be mistaken as crystals.

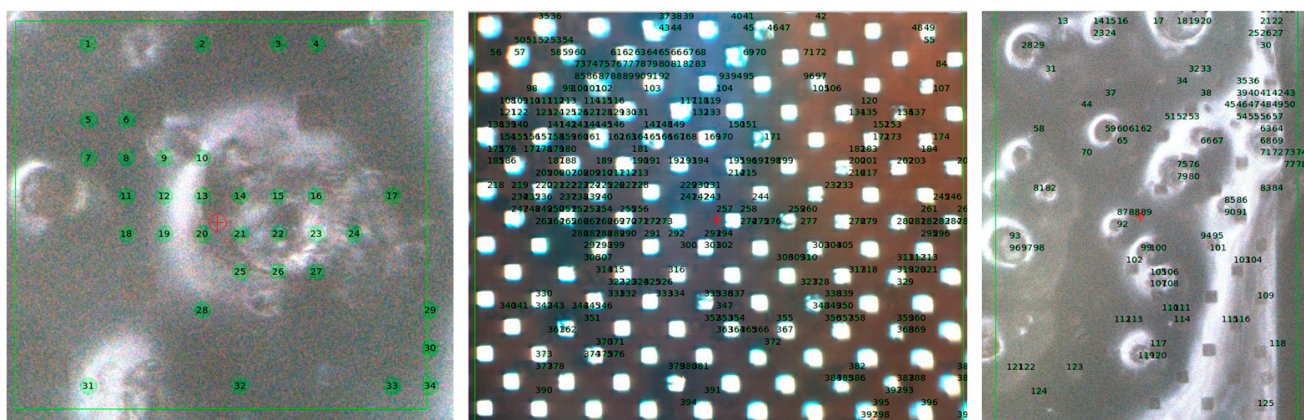


Figure 4. Three examples of the grids after the hit finding. The squares are the holes in the chips and the numbered green circles show the positions at which the crystal diffraction was determined using the peakfinder8 algorithm. The red circle with the cross represents the current beam position.

The speedup achieved through the proposed approach heavily relies on the concentration of crystals deposited on the chip. Comparing the fly scan to the step scan, the former proves to be significantly faster. For instance, a fly scan covering a 50×18 grid (900 positions) with a 40 ms exposure time and a $50 \mu\text{m}$ step completes in approximately 100 s. Out of this time, around 36 s are devoted to the actual data acquisition, while the remaining 1 min accounts for scan preparation, motor movement, and positioning. On the other hand, a step scan necessitates several seconds for positioning at each point, resulting in a scan with 900 points taking over 30 min. Scanning 545 preselected points with 11 frames per position took approximately 28 min. In addition, a step scan with 27 positions required only a few minutes to complete. This evident contrast highlights the immense advantage of investing some time in conducting a fast fly scan to determine the positions of the crystals.

To check if the positions of crystals on the chip were determined correctly, we performed the following test: the whole dataset measured during the low-dose fly scan was processed using CrystFEL [41] and the indexing results were compared to the result of processing a subset containing only hits found by the peakfinder8. In all cases, the indexing of the whole measured dataset led to the identical number of indexed crystals as the indexing of just the identified patterns. This suggests that measuring the positions where the crystals were not detected during the hit-finding step gives no additional information. The number of indexed crystals on several measured grids are presented in Table 1. Each grid consisted of 900 positions.

Table 1. Several scans of different loads of lysozyme samples on a chip. Every grid contained 900 positions (50×18).

Dataset	Number of Indexable Patterns	Compression Rate
Lyso1_grid1	27	33.3
Lyso1_grid2	94	9.6
Lyso2_grid1	232	3.8
Lyso3_grid1	545	1.7
Lyso4_grid1	511	1.8
Lyso5_grid1	155	5.8

The last column of Table 1 lists the ratio of the total number of recorded frames to the number of indexable frames. It is clear that our approach offers significant advantages, both in terms of time saved during data recording and the amount of data saved.

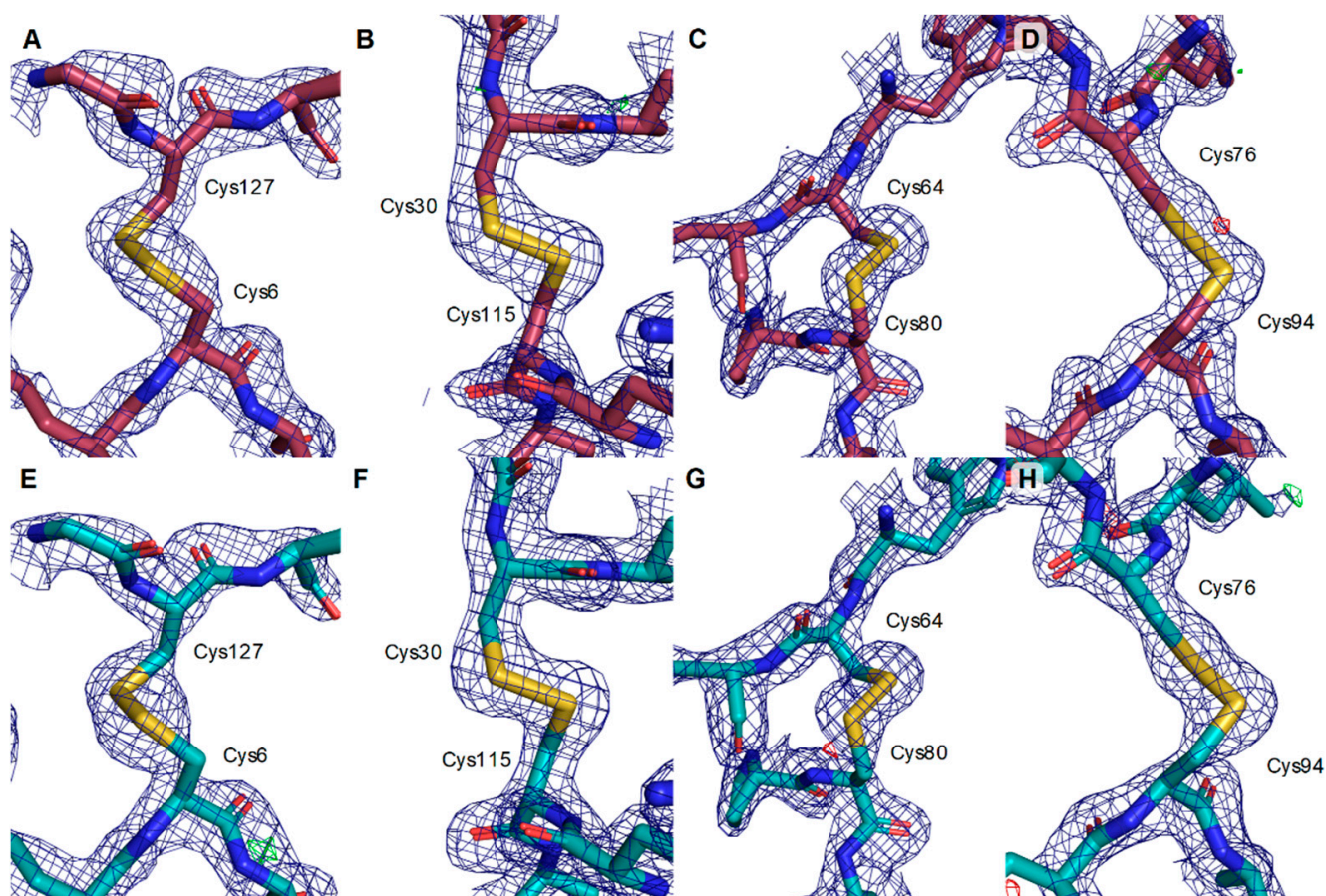
As described above, after the determination of the positions of the crystals inside the grid, the mini-rotation series were collected at each position determined as a hit. Such a dataset can be treated as serial data using CrystFEL—in this case, the fact that each rotation series was measured from one crystal was not considered. Alternatively, one can try to process each series independently using, for example, XDS and merge the integrated reflections obtained for different positions. While the first method is simpler for users, the second method might give better results since it solves the partiality problem within each rotation series. The optimization of processing the mini-rotation series is outside the scope of this paper, so it will be discussed in later publications.

To demonstrate that the measured data can be used for structure determination, we have processed data collected during two different experiments. The datasets were treated with consistent parameters during processing of raw data and during structure refinement (see the Methods section for details). The resulting statistics are summarized in Table 2.

Table 2. Overall statistics for two datasets collected during different chips after predetermination of exact crystal positions with low dose.

	Experiment 11013662	Experiment 11013278
Number of patterns	9230	15023
Indexed patterns/crystals	1899/2088	1189/1321
Resolution, Å	79.00–2.00 (2.03–2.0)	79.00–2.00 (2.03–2.0)
SNR	4.81 (1.36)	2.96 (0.33)
CC*	0.975 (0.603)	0.962 (0.284)
CC _{1/2}	0.907 (0.222)	0.860 (0.042)
R _{split} , %	26.82 (106.18)	35.97 (203.09)
Completeness, %	100.0 (100.0)	95.75 (75.12)
Multiplicity	59.08 (41.6)	16.25 (4.9)
Unique reflections	8589 (414)	8223 (311)
Wilson B-factor	28.03	28.18
R _{free} /R _{work}	0.29/0.27	0.28/0.27

Parts of the reconstructed structures are presented in Figure 5. Visual inspection of obtained electron density maps from both datasets did not reveal any indication of radiation damage.

**Figure 5.** Electron densities around the four disulfide bridges in the structures solved from two experiments: (A–D) 11013278 and (E–H) BT11013662. Blue mesh, 2Fo-Fc, 1.5 σ ; green/red mesh, Fo-Fc, $\pm 3 \sigma$; both carved at 1.6 Å around the depicted atoms.

4. Discussion

X-ray serial protein crystallography is under continued and intense development as a method to determine the structures of proteins without the need for cryogenic cooling. Because of rapid developments in such areas as detectors, sample preparation protocols, sample delivery systems, and optics, new strategies for data collection have appeared. Of the two main types of sample delivery systems, fixed-target methods offer several advantages over jet injectors, including lower sample consumption, clog-free delivery, often lower background, and the ability to control crystal-on-chip density for optimal hit rates. This work is focused on the optimization of the measurement of crystals deposited on fixed-target supports (chips) using a two-step scanning mode: first, the chip is scanned at a low dose and high speed to determine the positions of crystals on the chip. Only these positions are subsequently measured as mini rotation series. The determination of the crystal positions is conducted during the first fly scan and a grid of interesting positions is formed automatically. Although the low-dose scan may miss some weakly diffracting crystals that could give measurable signals with higher exposure, these weak crystals are unlikely to contribute to the overall result, especially if well-diffracting crystals are found. In cases where the experiment is aimed at the measuring diffraction from small crystals (for example, for time-resolved measurements), we suggest using some other strategy (for example, a series of fly scans at different inclination angles of the chip).

A potential future improvement of the methods involves analyzing the fly scan data to accurately determine the centers of the detected crystals, especially if they are larger than the step size of the scan. By measuring each crystal at its center, more representative and comprehensive data can be obtained. Furthermore, an optimal strategy would be to adjust the size of the beam based on the detected crystal's size, possibly by modifying the aperture. However, it is essential to consider that such improvements might require additional adjustments to the beamline hardware. Additionally, this approach might encounter difficulties when dealing with a high density of deposited crystals, where distinguishing individual crystal centers could become problematic.

In this paper, we acknowledge that the data processing of the mini-rotation using CrystFEL may not be optimal, as it disregards the additional information obtained from the rotation of the measured sample. As part of our future plans, we intend to enhance the pipeline by incorporating XDS along with XSCALE for processing the measured data. This modification aims to address the partiality problem and leverage the benefits of additional constraints provided by rotation. We intend to investigate the differences between the two methods in our future studies.

The method proposed in this study is versatile and applicable both at synchrotrons and laboratory sources. Using an attenuated beam, the method can be utilized at FELs for measurements of rapid dynamical processes, such as light-activated phenomena, in protein crystals. However, to address the partiality problem, the rotating increment has to be small (within the divergence and the bandwidth of the beam) due to the pulsed nature of the FELs. Additionally, it is worth noting that measuring using an attenuated beam of the FEL might not be the most optimal approach. Therefore, we recommend considering alternative measurement strategies for protein crystallography using FELs.

Optimizing the scanning process offers multiple benefits, including faster data collection and a reduction in data volume. By avoiding the collection of empty frames from crystal-lacking positions, unnecessary data are prevented from being stored, resulting in significant resource savings. In our tests, depending on the concentration of well-diffracted protein crystals on the chip, we were able to achieve storage savings ranging from 1.7 up to 33 times. The method exhibits its most significant improvement when the chip is loaded with only a few crystals, which is often the case for certain proteins that are particularly challenging to crystallize. In such instances, the proposed method becomes instrumental in maximizing the utilization of all available crystals, greatly enhancing the likelihood of successfully obtaining the structure of the measured protein.

The developed “smart” chip-scanning approach was implemented in a separate branch of the CrystalControl software at the P11 beamline and this approach can be easily integrated into the controlling software at other beamlines.

Author Contributions: Sample preparation, A.R.M. and P.Y.A.R.; software, M.G. and J.M.; experiment, M.G. and O.M.Y.; idea, M.G., O.M.Y. and H.N.C.; data processing, M.G. and O.M.Y.; writing, M.G.; editing, O.M.Y. and H.N.C.; chips, P.Y.A.R. and S.G. All authors have read and agreed to the published version of the manuscript.

Funding: This research was partially funded by the Helmholtz-Gemeinschaft through the projects FISCOV and SFRagX. (P.Y.A.R.) and the Helmholtz Association Impulse and Networking funds InternLabs-0011 “HIR3X”.

Data Availability Statement: Experimental data are stored at the Petra III facility for at least 5 years after the experiment. They are available upon a reasonable request to the authors.

Acknowledgments: The authors are thankful to the scientific staff from the P11 beamline at Petra III for allowing them to check and validate our ideas. This research was supported in part through the Maxwell computational resources operated at Deutsches Elektronen-Synchrotron DESY, Hamburg, Germany.

Conflicts of Interest: The authors declare no conflict of interest.

References

1. Garman, E.F. Radiation Damage in Macromolecular Crystallography: What Is It and Why Should We Care? *Acta Crystallogr. Sect. D Biol. Crystallogr.* **2010**, *66*, 339–351. [[CrossRef](#)]
2. Nass, K. Radiation Damage in Protein Crystallography at X-ray Free-Electron Lasers. *Acta Crystallogr. D Struct. Biol.* **2019**, *75*, 211–218. [[CrossRef](#)]
3. Brändén, G.; Neutze, R. Advances and Challenges in Time-Resolved Macromolecular Crystallography. *Science* **2021**, *373*, eaba0954. [[CrossRef](#)]
4. Chapman, H.N.; Fromme, P.; Barty, A.; White, T.A.; Kirian, R.A.; Aquila, A.; Hunter, M.S.; Schulz, J.; DePonte, D.P.; Weierstall, U.; et al. Femtosecond X-Ray Protein Nanocrystallography. *Nature* **2011**, *470*, 73–77. [[CrossRef](#)]
5. Boutet, S.; Lomb, L.; Williams, G.J.; Barends, T.R.M.; Aquila, A.; Doak, R.B.; Weierstall, U.; DePonte, D.P.; Steinbrener, J.; Shoeman, R.L.; et al. High-Resolution Protein Structure Determination by Serial Femtosecond Crystallography. *Science* **2012**, *337*, 362–364. [[CrossRef](#)]
6. Stellato, F.; Oberthür, D.; Liang, M.; Bean, R.; Gati, C.; Yefanov, O.; Barty, A.; Burkhardt, A.; Fischer, P.; Galli, L.; et al. Room-Temperature Macromolecular Serial Crystallography Using Synchrotron Radiation. *IUCr* **2014**, *1*, 204–212. [[CrossRef](#)]
7. Gati, C.; Bourenkov, G.; Klinge, M.; Rehders, D.; Stellato, F.; Oberthür, D.; Yefanov, O.; Sommer, B.P.; Mogk, S.; Duszynko, M.; et al. Serial Crystallography on in Vivo Grown Microcrystals Using Synchrotron Radiation. *IUCr* **2014**, *1*, 87–94. [[CrossRef](#)]
8. Schmidt, M. Time-Resolved Macromolecular Crystallography at Pulsed X-ray Sources. *Int. J. Mol. Sci.* **2019**, *20*, 1401. [[CrossRef](#)]
9. Schmidt, M. Reaction Initiation in Enzyme Crystals by Diffusion of Substrate. *Crystals* **2020**, *10*, 116. [[CrossRef](#)]
10. Grünbein, M.L.; Nass Kovacs, G. Sample Delivery for Serial Crystallography at Free-Electron Lasers and Synchrotrons. *Acta Crystallogr. D Struct. Biol.* **2019**, *75*, 178–191. [[CrossRef](#)]
11. Zhao, F.; Zhang, B.; Yan, E.; Sun, B.; Wang, Z.; He, J.; Yin, D. A Guide to Sample Delivery Systems for Serial Crystallography. *FEBS J.* **2019**, *286*, 4402–4417. [[CrossRef](#)]
12. DePonte, D.P.; Weierstall, U.; Schmidt, K.; Warner, J.; Starodub, D.; Spence, J.C.H.; Doak, R.B. Gas Dynamic Virtual Nozzle for Generation of Microscopic Droplet Streams. *J. Phys. D Appl. Phys.* **2008**, *41*, 195505. [[CrossRef](#)]
13. Oberthuer, D.; Knoška, J.; Wiedorn, M.O.; Beyerlein, K.R.; Bushnell, D.A.; Kovaleva, E.G.; Heymann, M.; Gumprecht, L.; Kirian, R.A.; Barty, A.; et al. Double-Flow Focused Liquid Injector for Efficient Serial Femtosecond Crystallography. *Sci. Rep.* **2017**, *7*, 44628. [[CrossRef](#)]
14. Weierstall, U.; James, D.; Wang, C.; White, T.A.; Wang, D.; Liu, W.; Spence, J.C.H.; Bruce Doak, R.; Nelson, G.; Fromme, P.; et al. Lipidic Cubic Phase Injector Facilitates Membrane Protein Serial Femtosecond Crystallography. *Nat. Commun.* **2014**, *5*, 3309. [[CrossRef](#)]
15. Henkel, A.; Maracke, J.; Munke, A.; Galchenkova, M.; Rahmani Mashhour, A.; Reinke, P.; Domaracky, M.; Fleckenstein, H.; Hakanpää, J.; Meyer, J.; et al. CFEL TapeDrive 2.0: A Conveyor Belt-Based Sample-Delivery System for Multi-Dimensional Serial Crystallography. *Acta Crystallogr. A Found. Adv.* **2022**, *78*, e560. [[CrossRef](#)]
16. Hunter, M.S.; Segelke, B.; Messerschmidt, M.; Williams, G.J.; Zatsepin, N.A.; Barty, A.; Benner, W.H.; Carlson, D.B.; Coleman, M.; Graf, A.; et al. Fixed-Target Protein Serial Microcrystallography with an x-Ray Free Electron Laser. *Sci. Rep.* **2014**, *4*, 6026. [[CrossRef](#)]

17. Mueller, C.; Marx, A.; Epp, S.W.; Zhong, Y.; Kuo, A.; Balo, A.R.; Soman, J.; Schotte, F.; Lemke, H.T.; Owen, R.L.; et al. Fixed Target Matrix for Femtosecond Time-Resolved and in Situ Serial Micro-Crystallography. *Struct. Dyn.* **2015**, *2*, 054302. [[CrossRef](#)]
18. Roedig, P.; Vartiainen, I.; Duman, R.; Panneerselvam, S.; Stübe, N.; Lorbeer, O.; Warmer, M.; Sutton, G.; Stuart, D.I.; Weckert, E.; et al. A Micro-Patterned Silicon Chip as Sample Holder for Macromolecular Crystallography Experiments with Minimal Background Scattering. *Sci. Rep.* **2015**, *5*, 10451. [[CrossRef](#)]
19. Oghbaey, S.; Sarracini, A.; Ginn, H.M.; Pare-Labrosse, O.; Kuo, A.; Marx, A.; Epp, S.W.; Sherrell, D.A.; Eger, B.T.; Zhong, Y.; et al. Fixed Target Combined with Spectral Mapping: Approaching 100% Hit Rates for Serial Crystallography. *Acta Crystallogr. D Struct. Biol.* **2016**, *72*, 944–955. [[CrossRef](#)]
20. Owen, R.L.; Axford, D.; Sherrell, D.A.; Kuo, A.; Ernst, O.P.; Schulz, E.C.; Miller, R.J.D.; Mueller-Werkmeister, H.M. Low-Dose Fixed-Target Serial Synchrotron Crystallography. *Acta Crystallogr. D Struct. Biol.* **2017**, *73*, 373–378. [[CrossRef](#)]
21. Kisselman, G.; Qiu, W.; Romanov, V.; Thompson, C.M.; Lam, R.; Battaile, K.P.; Pai, E.F.; Chirgadze, N.Y. X-CHIP: An Integrated Platform for High-Throughput Protein Crystallization and on-the-Chip X-Ray Diffraction Data Collection. *Acta Crystallogr. D Biol. Crystallogr.* **2011**, *67*, 533–539. [[CrossRef](#)]
22. Roedig, P.; Ginn, H.M.; Pakendorf, T.; Sutton, G.; Harlos, K.; Walter, T.S.; Meyer, J.; Fischer, P.; Duman, R.; Vartiainen, I.; et al. High-Speed Fixed-Target Serial Virus Crystallography. *Nat. Methods* **2017**, *14*, 805–810. [[CrossRef](#)]
23. Meents, A.; Wiedorn, M.O.; Srajer, V.; Henning, R.; Sarrou, I.; Bergtholdt, J.; Barthelmess, M.; Reinke, P.Y.A.; Dierksmeyer, D.; Tolstikova, A.; et al. Pink-Beam Serial Crystallography. *Nat. Commun.* **2017**, *8*, 1281. [[CrossRef](#)]
24. Park, S.-Y.; Choi, H.; Eo, C.; Cho, Y.; Nam, K.H. Fixed-Target Serial Synchrotron Crystallography Using Nylon Mesh and Enclosed Film-Based Sample Holder. *Crystals* **2020**, *10*, 803. [[CrossRef](#)]
25. Gilbille, D.; Shelby, M.L.; Lyubimov, A.Y.; Wierman, J.L.; Monteiro, D.C.F.; Cohen, A.E.; Russi, S.; Coleman, M.A.; Frank, M.; Kuhl, T.L. Plug-and-Play Polymer Microfluidic Chips for Hydrated, Room Temperature, Fixed-Target Serial Crystallography. *Lab Chip* **2021**, *21*, 4831–4845. [[CrossRef](#)]
26. Lee, K.Y. Micromachining Applications of a High Resolution Ultrathick Photoresist. *J. Vac. Sci. Technol. B* **1995**, *13*, 3012. [[CrossRef](#)]
27. Lieske, J.; Cerv, M.; Kreida, S.; Komadina, D.; Fischer, J.; Barthelmess, M.; Fischer, P.; Pakendorf, T.; Yefanov, O.; Mariani, V.; et al. On-Chip Crystallization for Serial Crystallography Experiments and on-Chip Ligand-Binding Studies. *IUCr* **2019**, *6*, 714–728. [[CrossRef](#)]
28. Wierman, J.L.; Paré-Labrosse, O.; Sarracini, A.; Besaw, J.E.; Cook, M.J.; Oghbaey, S.; Daoud, H.; Mehrabi, P.; Kriksunov, I.; Kuo, A.; et al. Fixed-Target Serial Oscillation Crystallography at Room Temperature. *IUCr* **2019**, *6*, 305–316. [[CrossRef](#)]
29. Asanov, A.N.; McDonald, H.M.; Oldham, P.B.; Jedrzejak, M.J.; Wilson, W.W. Intrinsic Fluorescence as a Potential Rapid Scoring Tool for Protein Crystals. *J. Cryst. Growth* **2001**, *232*, 603–609. [[CrossRef](#)]
30. Chavas, L.M.G.; Yamada, Y.; Hiraki, M.; Igarashi, N.; Matsugaki, N.; Wakatsuki, S. UV LED Lighting for Automated Crystal Centring. *J. Synchrotron Radiat.* **2011**, *18*, 11–15. [[CrossRef](#)]
31. Vernede, X.; Lavault, B.; Ohana, J.; Nurizzo, D.; Joly, J.; Jacquamet, L.; Felisaz, F.; Cipriani, F.; Bourgeois, D. UV Laser-Excited Fluorescence as a Tool for the Visualization of Protein Crystals Mounted in Loops. *Acta Crystallogr. D Biol. Crystallogr.* **2006**, *62*, 253–261. [[CrossRef](#)]
32. Bourgeois, D.; Vernede, X.; Adam, V.; Fioravanti, E.; Ursby, T. A Microspectrophotometer for UV–Visible Absorption and Fluorescence Studies of Protein Crystals. *J. Appl. Crystallogr.* **2002**, *35*, 319–326. [[CrossRef](#)]
33. Kissick, D.J.; Dettmar, C.M.; Becker, M.; Mulichak, A.M.; Cherezov, V.; Ginell, S.L.; Battaile, K.P.; Keefe, L.J.; Fischetti, R.F.; Simpson, G.J. Towards Protein-Crystal Centering Using Second-Harmonic Generation (SHG) Microscopy. *Acta Crystallogr. D Biol. Crystallogr.* **2013**, *69*, 843–851. [[CrossRef](#)]
34. Murray, T.D.; Lyubimov, A.Y.; Ogata, C.M.; Vo, H.; Uervirojnangkoorn, M.; Brunger, A.T.; Berger, J.M. A High-Transparency, Micro-Patternable Chip for X-Ray Diffraction Analysis of Microcrystals under Native Growth Conditions. *Acta Crystallogr. D Biol. Crystallogr.* **2015**, *71*, 1987–1997. [[CrossRef](#)]
35. Burkhardt, A.; Pakendorf, T.; Reime, B.; Meyer, J.; Fischer, P.; Stübe, N.; Panneerselvam, S.; Lorbeer, O.; Stachnik, K.; Warmer, M.; et al. Status of the Crystallography Beamlines at PETRA III. *Eur. Phys. J. Plus* **2016**, *131*, 56. [[CrossRef](#)]
36. Barty, A.; Kirian, R.A.; Maia, F.R.N.C.; Hantke, M.; Yoon, C.H.; White, T.A.; Chapman, H. *Cheetah*: Software for High-Throughput Reduction and Analysis of Serial Femtosecond X-Ray Diffraction Data. *J. Appl. Crystallogr.* **2014**, *47*, 1118–1131. [[CrossRef](#)] [[PubMed](#)]
37. Zander, U.; Bourenkov, G.; Popov, A.N.; de Sanctis, D.; Svensson, O.; McCarthy, A.A.; Round, E.; Gordeliy, V.; Mueller-Dieckmann, C.; Leonard, G.A. *MeshAndCollect*: An Automated Multi-Crystal Data-Collection Workflow for Synchrotron Macromolecular Crystallography Beamlines. *Acta Crystallogr. D Biol. Crystallogr.* **2015**, *71*, 2328–2343. [[CrossRef](#)]
38. de la Mora, E.; Coquelle, N.; Bury, C.S.; Rosenthal, M.; Holton, J.M.; Carmichael, I.; Garman, E.F.; Burghammer, M.; Colletier, J.-P.; Weik, M. Radiation Damage and Dose Limits in Serial Synchrotron Crystallography at Cryo- and Room Temperatures. *Proc. Natl. Acad. Sci. USA* **2020**, *117*, 4142–4151. [[CrossRef](#)]
39. Gevorkov, Y.; Yefanov, O.; Barty, A.; White, T.A.; Mariani, V.; Brehm, W.; Tolstikova, A.; Grigat, R.-R.; Chapman, H.N. XGANDALF—Extended Gradient Descent Algorithm for Lattice Finding. *Acta Crystallogr. Sect. A Found. Adv.* **2019**, *75*, 694–704. [[CrossRef](#)]

40. Adams, P.D.; Afonine, P.V.; Bunkóczy, G.; Chen, V.B.; Davis, I.W.; Echols, N.; Headd, J.J.; Hung, L.-W.; Kapral, G.J.; Grosse-Kunstleve, R.W.; et al. *PHENIX : A Comprehensive Python-Based System for Macromolecular Structure Solution*. *Acta Crystallogr. D Biol. Crystallogr.* **2010**, *66*, 213–221. [[CrossRef](#)]
41. White, T.A.; Kirian, R.A.; Martin, A.V.; Aquila, A.; Nass, K.; Barty, A.; Chapman, H.N. *CrystFEL : A Software Suite for Snapshot Serial Crystallography*. *J. Appl. Crystallogr.* **2012**, *45*, 335–341. [[CrossRef](#)]

Disclaimer/Publisher’s Note: The statements, opinions and data contained in all publications are solely those of the individual author(s) and contributor(s) and not of MDPI and/or the editor(s). MDPI and/or the editor(s) disclaim responsibility for any injury to people or property resulting from any ideas, methods, instructions or products referred to in the content.